SCIENCE CHINA
Information Sciences

• RESEARCH PAPER •

July 2026, Vol. 69, Iss. 7, 172204:1–172204:14
https://doi.org/10.1007/s11432-024-4886-7

Fault-tolerant control for switched nonlinear systems with multichannel actuators and deferred constraints via a learning-based switching mechanism

Wei QIAN[1,2*], Quan WAN[1,2] & Bo SHEN[3]

[1]*School of Electrical Engineering and Automation, Henan Polytechnic University, Jiaozuo 454000, China*
[2]*Henan Key Laboratory of Intelligent Detection and Control of Coal Mine Equipment, Henan Polytechnic University, Jiaozuo 454000, China*
[3]*College of Information Science and Technology, Donghua University, Shanghai 201620, China*

Received 12 December 2024/Revised 14 April 2025/Accepted 14 July 2025/Published online 26 May 2026

Abstract This study proposes an improved adaptive fault-tolerant control (FTC) scheme for switched nonlinear systems with multichannel actuators and deferred constraints. First, a novel multivariable lemma for type-B Nussbaum functions is developed, in which the monotonicity requirement on the Nussbaum argument is removed under time-varying gains. Second, inspired by the concept of deferred constraints, an enhanced tracking control method is proposed, which achieves excellent tracking performance without imposing strict initial conditions. Specifically, the tracking error rapidly converges to a specified region within a preset time without noticeable overshoot and asymptotically converges to zero. Third, a new fault-tolerant controller is designed, which consists of a control protocol and a learning-based switching mechanism. Finally, the proposed mechanism enables fault detection and automatic switching of working modes without human intervention in a reasonably efficient manner. The proposed FTC architecture does not need an additional fault detection and/or isolation unit, reducing the risk of false and missed alarms. Moreover, the simplified design framework avoids filtering techniques and prevents an "explosion of complexity". All closed-loop signals are proven to be semiglobally uniformly ultimately bounded (SUUB) under arbitrary switching, and excellent tracking performance is realized. Simulation results confirm the superiority of the proposed control method.

Keywords switched nonlinear systems, fault-tolerant control (FTC), deferred constraints, Nussbaum function, actuator faults

Citation Qian W, Wan Q, Shen B. Fault-tolerant control for switched nonlinear systems with multichannel actuators and deferred constraints via a learning-based switching mechanism. Sci China Inf Sci, 2026, 69(7): 172204, https://doi.org/10.1007/s11432-024-4886-7

1 Introduction

Given the favorable characteristic of sophisticated engineering objects (e.g., mechanical and electrohydraulic systems) that can be modeled as switched nonlinear systems, research results [1–5] on control issues revolving around switched nonlinear systems have recently proliferated, in which the challenging unknown nonlinear portions were addressed by linear parameterization of the approximators, such as fuzzy logic systems [6–8] and neural networks (NNs) [9–11]. Furthermore, *a priori* knowledge of control gain is frequently hard to access. The Nussbaum gain technique [12–14], as an effective means, was utilized to resolve the issue of unknown constant and/or time-varying control gains for switched nonlinear systems. Yet, Chen [15] identified the important concern that general Nussbaum functions are not valid for certain time-varying gains and defined the type-B Nussbaum function, which can handle all time-varying gain functions. However, there exists a conservative condition for the arguments of the Nussbaum function to be monotonically increasing with positive initial values. Thereafter, Hua et al. [16] relaxed this rigid condition, i.e., all the arguments need only be monotonic (note that the monotonicity condition remains).

In addition, the objects to be controlled in the operational environments commonly need to fulfill specific performance index requirements, such as convergence speed/settling time, overshoot, and steady-state error. Consequently, performance constraint control (PCC) methods [17–20] have been developed and refined. For example, the tunnel prescribed performance (TPP) with a compact form and smaller overshoot was realized in [19]. Wang and Long [20] achieved fast convergence performance of the tracking error within a predefined funnel with the ideas of funnel control. Nevertheless, all of the foregoing methods require relatively stringent initial conditions. To

* Corresponding author (email: qwei@hpu.edu.cn)

resolve this issue, recent results [21–24] have been presented in succession. For instance, Ji et al. [23] solved the entry capture issue on the basis of scaling and self-tuning functions to guarantee TPP with an arbitrary tracking error. The preset-time and preset-accuracy cluster consensus control was achieved in [24] without initial condition limitations.

From another perspective, system operation is inevitably subject to unpredictable faults, considering the impact of component aging and environmental factors. Thus, studies on maintaining system performance or robustness through various fault-tolerant control (FTC) designs [25–36] have been extensively conducted. One of the FTC ideas [29–31] involves designing a fault detection and isolation (FDI) unit to detect anomalous residual signals and isolate faults, followed by controller reconfiguration to mitigate fault effects. However, the constructed FDI unit raises the complication of the control structure and the risk of missed alarms. Additionally, actuator faults, as a common type of fault, may cause reconfigurable controller designs to be ineffective. To respond effectively to this fault scenario, a category of FTC solutions (e.g., [33, 34]) for providing redundant actuators as alternatives was proposed to replace the faulty actuator promptly. These solutions, however, still require the construction of fault detection units to obtain the exact instant of switching to the alternative actuator. To relax this concern, Yang et al. [35] designed a novel adaptive learning-based FTC scheme for nonlinear systems. Afterwards, the FTC issue with performance constraints was studied in [36] using a learning-based switching mechanism.

Considering the above findings, the following three important questions naturally arise.

(I) Can the monotonicity condition for multiple arguments of type-B Nussbaum functions be removed?

(II) Can tracking performance be further improved by performance constraints without strict initial conditions?

(III) Can fault detection and accommodation behavior be optimized via a learning-based switching mechanism?

The answers to these questions are obtained by providing a new adaptive FTC design solution for switched nonlinear systems. The main contributions are enumerated below.

(1) Through an analysis based on interval segmentation and mathematical induction, a new multivariable lemma for type-B Nussbaum functions is given to handle the unknown gains. The monotonicity condition [15, 16] for multiple arguments of type-B Nussbaum functions is removed in the given lemma, which relaxes the restrictions on control design.

(2) An improved tracking control method with deferred constraints is proposed, which offers four advantages. (i) The strict initial conditions for tracking error in the PCC methods [17–20] are eliminated. (ii) Superior transient performance without significant overshoot is realized. (iii) Fast convergence performance is realized, in which the settling time and convergence region can be arbitrarily adjusted according to user requirements. (iv) Asymptotic tracking performance is realized.

(3) According to a new update protocol of the switching performance index, a learning-based switching mechanism is designed to address actuator faults, which monitors the error signal in real time and rapidly switches the actuator working mode without human intervention when the abnormal error signal appears until the signal returns to normal. Compared with the analogous mechanism [36], the proposed mechanism optimizes fault detection and accommodation behavior, i.e., relaxes the initial detection baseline and reduces frequent and unnecessary switching times in the initial period.

(4) A simplified yet feasible design framework is formulated by ingenious NN-based scaling, which removes the assumption of *a priori* knowledge of high-order derivatives of the reference signal being known and averts an "explosion of complexity" without using a dynamic surface or command filtering technique.

Notations. $\mathbb{R}^n$ represents the n-dimensional real space. $\mathrm{mod}(\cdot)$ denotes the residual operator. Ω_λ indicates a compact set about λ. $\lfloor\cdot\rfloor$ denotes the floor function. The arguments of certain functions are omitted.

2 Problem formulation and preliminaries

2.1 System description

Consider the switched nonlinear systems with multichannel actuators modeled below:

$$\begin{cases} \dot{x}_i = g_{i,\sigma}(\bar{x}_i, t)x_{i+1} + f_{i,\sigma}\left(\bar{x}_i\right), \ i = 1, 2, \ldots, n-1, \\ \dot{x}_n = \sum\limits_{c=1}^{M} g_{n,\sigma}^{c}(t)u_\sigma^c + f_{n,\sigma}\left(\bar{x}_n\right), \\ y = x_1, \end{cases} \tag{1}$$

where $\bar{x}_i = [x_1, \ldots, x_i]^{\mathrm{T}} \in \mathbb{R}^i$ $(i = 1, \ldots, n)$, $u_\sigma = [u_\sigma^1, \ldots, u_\sigma^M]^{\mathrm{T}} \in \mathbb{R}^M$, and $y \in \mathbb{R}$ are the state vector, input vector, and output signal, respectively. $\sigma : [0, \infty) \to \Pi = \{1, \ldots, I\}$ denotes the switching signal, where I represents the number of subsystems, and suppose that system states do not jump at switching instants. $f_{i,\sigma}(\bar{x}_i) \in \mathbb{R}$ are unknown yet smooth nonlinear functions. $g_{i,\sigma}(\bar{x}_i, t) \in \mathbb{R}$ and $g_{n,\sigma}(t) = [g_{n,\sigma}^1(t), \ldots, g_{n,\sigma}^M(t)] \in \mathbb{R}^M$ are unknown control gains.

Initially, the healthy system (1) can normally perform the specified control task. That is, the output signal y can well track the known bounded reference trajectory y_r, in which the time differential of y_r is known and bounded. Note that *a priori* knowledge of high-order differentials of y_r in [37,38] is not required. Yet, considering the impact of several internal and external factors, actuator fault may occur on a single channel or multiple channels in the subsequent time period, resulting in inaccurate transmission of the control signal to the system. Thus, the system input signal or actuator output signal of the cth channel u_σ^c can be represented as $u_\sigma^c = \vartheta_\sigma^c(q_c(t)v_\sigma^c(t), t)$, where the time-varying switching function $q_c(\cdot) : [0, \infty) \to \{0, 1\}$ denotes the virtual switch of the control protocol $v_\sigma^c(t)$, and the switch status can be determined instantly through software settings. In accordance with actuator fault models [39], actuator output signal u_σ^c can be further expressed below:

$$\begin{aligned} u_\sigma^c &= (1 - \beta_\sigma^c)\rho_\sigma^c q_c(t) v_\sigma^c(t) + \beta_\sigma^c \bar{u}_\sigma^c \\ &= \sum_{c \in \bar{\Phi}_l} \rho_\sigma^c q_c(t) v_\sigma^c(t) + \sum_{c \in \Phi_l} \bar{u}_\sigma^c, \end{aligned} \tag{2}$$

where $\beta_\sigma^c \in \{0, 1\}$, $\rho_\sigma^c \in (0, 1]$, and $\bar{u}_\sigma^c \in \mathbb{R}$ indicate characteristic parameters of different actuator operation patterns. Φ_l and $\bar{\Phi}_l$ represent the sets defined later. The following are three general actuator operation patterns.

• Total loss of effectiveness (TLOE). The output signal u_σ^c is independent of the actuator input signal and maintains a fixed value input to the system, i.e., $\beta_\sigma^c = 1$ and $\bar{u}_\sigma^c \in \mathbb{R}$.

• Partial loss of effectiveness (PLOE). The fault affects the normal signal transmission, resulting in the weakness of the transmitted signal u_σ^c, i.e., $\beta_\sigma^c = 0$ and $\rho_\sigma^c \in (0, 1)$.

• Fault-free (FF). The operation of the actuator does not affect the normal signal transmission, i.e., $\beta_\sigma^c = 0$ and $\rho_\sigma^c = 1$.

Problem statement. For the switched nonlinear systems (1) with multichannel actuators and deferred constraints, the control issue involves designing an adaptive FTC scheme such that

(1) All closed-loop signals are semiglobally uniformly ultimately bounded (SUUB) under arbitrary switching;

(2) Actuator faults in various scenarios can be timely detected and accommodated;

(3) The tracking error, under no initial restrictions, converges to the adjustable region without obvious overshoots in a preset time and asymptotically reaches zero.

Definition 1. There exist s TLOE patterns for M actuator channels, and the overall TLOE pattern set is defined as $\Psi := \{\Phi_1, \Phi_2, \ldots, \Phi_s\}$, where $\Phi_l = \{\Phi_{l1}, \Phi_{l2}, \ldots, \Phi_{l\mu_l}\}$ $(l \in \{1, 2, \ldots, s\})$ indicates the current TLOE pattern. Specifically, $\Phi_{l1}, \Phi_{l2}, \ldots, \Phi_{l\mu_l} \in \{1, 2, \ldots, M\}$ denote the channel serial numbers of the TLOE actuator, in which μ_l represents the sum of channels of the TLOE actuator. Thereafter, the complement of Φ_l is expressed as $\bar{\Phi}_l$ satisfying $\Phi_l \cup \bar{\Phi}_l = \{1, 2, \ldots, M\}$.

Assumption 1. The unknown time-varying gains satisfy $g_{i,\sigma}(\cdot) \in [\overline{g}, \underline{g}]$ $(i = 1, \ldots, n)$ with $\overline{g}\underline{g} > 0$.

Assumption 2. Only actuators with a maximum of $M - 1$ channels are allowed to undergo TLOE.

Remark 1. Assumption 1 is a basic necessary condition for using a Nussbaum-type function to handle the unknown control gains issue, which can be seen in [12–16]. Assumption 2 is a conservative premise for FTC methods for ensuring system controllability.

Lemma 1 ([40])**.** For any $\upsilon \in \mathbb{R}$ and time-varying function $\hbar(t) > 0$, it holds that

$$|\upsilon| - \frac{\upsilon^2}{\sqrt{\upsilon^2 + \hbar(t)^2}} \leqslant \hbar(t). \tag{3}$$

2.2 Nussbaum function

Definition 2 ([16])**.** A continuous function $\mathcal{N}(\xi) : [0, +\infty) \to (-\infty, +\infty)$ is defined as a type-B Nussbaum function if

$$\lim_{\xi \to +\infty} \frac{\int_0^\xi \mathcal{N}^+(\tau)d\tau}{\xi} = +\infty, \lim_{\xi \to +\infty} \sup \frac{\int_0^\xi \mathcal{N}^+(\tau)d\tau}{\int_0^\xi \mathcal{N}^-(\tau)d\tau} = +\infty,$$

$$\lim_{\xi\to+\infty}\frac{\int_0^\xi \mathcal{N}^-(\tau)d\tau}{\xi}=+\infty,\ \lim_{\xi\to+\infty}\sup\frac{\int_0^\xi \mathcal{N}^-(\tau)d\tau}{\int_0^\xi \mathcal{N}^+(\tau)d\tau}=+\infty,$$

where positive and negative truncated functions of $\mathcal{N}(\tau)$ are $\mathcal{N}^+(\tau)=\max\{0,\mathcal{N}(\tau)\}$ and $\mathcal{N}^-(\tau)=\max\{0,-\mathcal{N}(\tau)\}$, respectively.

Lemma 2. Consider continuously differentiable functions $V(t):[0,+\infty)\to\mathbb{R}^+$ and $\xi_i(t):[0,+\infty)\to\mathbb{R}$ $(i=1,2,\ldots,n)$. Let $g_i(t):[0,+\infty)\to[\overline{g},\underline{g}]$ with $\overline{g}\underline{g}>0$. If

$$V(t)\leqslant\sum_{i=1}^n\int_0^t(g_i(\tau)\mathcal{N}(\xi_i(\tau))+\kappa)\dot{\xi}_i(\tau)d\tau+b, \tag{4}$$

where κ and b are constants and $\mathcal{N}(\xi_i(t))$ denotes a composite function with $\mathcal{N}(\xi_i)$ being a type-B Nussbaum odd function, then $\xi_i(t)$, $V(t)$, and $\sum_{i=1}^n\int_0^t(g_i(\tau)\mathcal{N}(\xi_i(\tau))+\kappa)\dot{\xi}_i(\tau)d\tau\in\mathcal{L}_\infty$ hold for $t\in[0,+\infty)$.

Proof. See Appendix A.

Remark 2. The work [15] proved that only type-B Nussbaum functions are always effective for addressing the time-varying gains issue. With multiple time-varying gains, however, there are strict restrictions on the arguments $\xi_i(t)$ $(i=1,2,\ldots,n)$ of type-B Nussbaum functions in recent studies, i.e., all $\xi_i(t)$ must be monotonically increasing in [15] and all $\xi_i(t)$ must be monotonic in [16]. These restrictions are successfully removed by the proposed Lemma 2, which does not require the prerequisite of monotonicity of $\xi_i(t)$.

2.3 Neural networks

Definition 3 ([11])**.** For an unknown yet smooth nonlinear function $F(\chi):\mathbb{R}^p\to\mathbb{R}^q$ and the activation vector $\chi\in\Omega_\chi\subset\mathbb{R}^p$, there exists a radial basis function neural network (RBFNN) such that $F_\chi=\Xi^{\mathrm{T}}\varrho(\chi)+\delta(\chi)$ in which $\Xi\in\mathbb{R}^{j\times q}$ denotes the idealized weight matrix. $\delta(\chi)$ represents the approximation error with $\|\delta(\chi)\|\leqslant\bar{\delta}$ for constant $\bar{\delta}$. j is the node number of the NN. $\varrho(\chi)=[\varrho_1(\chi),\ldots,\varrho_j(\chi)]^{\mathrm{T}}\in\mathbb{R}^{j\times q}$ is the Gaussian basis function vector, where $\varrho_i(\chi)=\exp(-(\chi-c_i)^{\mathrm{T}}(\chi-c_i)/d_i^2)$ with $c_i=[c_{i1},\ldots,c_{ip}]^{\mathrm{T}}$ and d_i being the center and width of the Gaussian function, respectively.

Lemma 3 ([11])**.** For the Gaussian basis function vector $\varrho(\chi_{\bar{l}})=[\varrho_1(\chi_{\bar{l}}),\ldots,\varrho_j(\chi_{\bar{l}})]^{\mathrm{T}}\in\mathbb{R}^{j\times q}$ and the activation vector $\chi_{\bar{l}}=[\chi_1^*,\ldots,\chi_{\bar{l}}^*]^{\mathrm{T}}\in\mathbb{R}^{\bar{l}}$, given any positive integer $\bar{l}\leqslant\bar{m}$, one has $\|\varrho(\chi_{\bar{m}})\|\leqslant\|\varrho(\chi_{\bar{l}})\|$.

Remark 3. Lemma 3 embodies an applicable RBFNN characteristic, allowing designers to eliminate some fussy and redundant variables from the activation input χ while maintaining its approximate property, which can significantly simplify the NN-based design process and control structure.

3 Adaptive control design scheme

In this section, an adaptive FTC scheme based on a backstepping procedure for switched nonlinear systems with multichannel actuators and deferred constraints is presented. A schematic of the control design is shown in Figure 1.

3.1 Deferred constraints control design

The given tracking error is $e_1=x_1-y_r$. Use the idea of deferred constraints to perform fine-tuning on e_1. The tuned error $\tilde{e}_1$ is defined as $\tilde{e}_1(t)=r(t)e_1(t)+o(t)$ and $\tilde{e}_1=e_1(t\geqslant T_D)$, where the switching function $r(t)$ is expressed as

$$r(t)=\begin{cases}\exp\left(-\frac{(t-T_D)^2}{\Delta}\right), & 0\leqslant t<T_D,\\ 1, & t\geqslant T_D,\end{cases} \tag{5}$$

where T_D is the deferred time, and Δ is a constant with $0<\Delta\ll1$. $o(t)$ is an initial-error-dependent function defined later.

The constraint feasible region of $\tilde{e}_1$ is designated as $\mathcal{F}:=\{(t,\tilde{e}_1)\in\mathbb{R}_{\geqslant0}\times\mathbb{R}|-q_l(t)<\tilde{e}_1(t)<q_h(t)\}$, where $q_l(t)=q_{T_s}\mathrm{sign}(e_1(0))+(\varepsilon_l-\mathrm{sign}(e_1(0)))q(t)$ and $q_h(t)=-q_{T_s}\mathrm{sign}(e_1(0))+(\varepsilon_h+\mathrm{sign}(e_1(0)))q(t)$, in which $\varepsilon_l,\varepsilon_h\in$

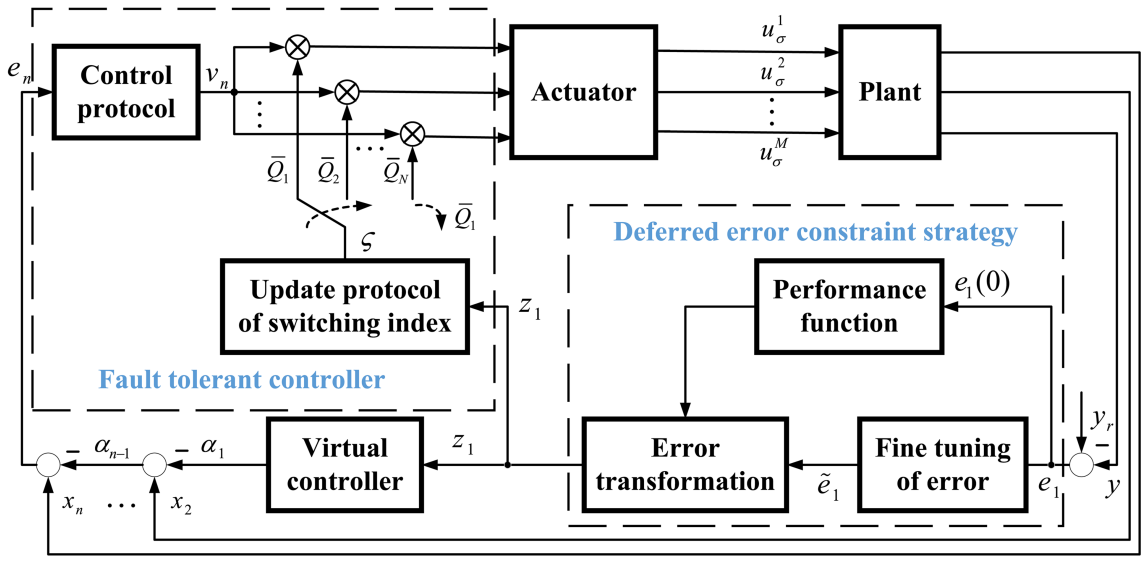

Figure 1 (Color online) Schematic of the FTC design with deferred constraints.

$(0, 1]$ and $q(t)$ is defined as

$$q(t) = \begin{cases} (q_0 - q_{T_s}) \left(1 - \frac{\nu t}{p}\right)^p + q_{T_s}, & 0 \leqslant t < T_s, \\ q_{T_s}, & t \geqslant T_s, \end{cases} \tag{6}$$

where $p > 1$, $q_0 > q_{T_s}$ and ν are positive constants. T_s represents the preset time meeting $T_s = p/\nu > T_D$.

Remark 4. For the case of $e_1(0) \neq 0$, the monotonic constraint functions satisfy the following properties. (i) $\lim_{t\to T_s} q_l(t) = \varepsilon_l q_{T_s}$ and $\lim_{t\to T_s} q_h(t) = \varepsilon_h q_{T_s}$. (ii) $q_l(t) = \varepsilon_l q_{T_s} (t \geqslant T_s)$ and $q_h(t) = \varepsilon_h q_{T_s} (t \geqslant T_s)$. (iii) $\dot{q}_l(t)\dot{q}_h(t) \leqslant 0$. (iv) $q_l(t) + q_h(t) > 0$. $-q_l(t)$ and $q_h(t)$ are known to converge quickly from the same direction to their respective fixed levels, thus generating a tight feasible region $\mathcal{F}$. The constrained $\tilde{e}_1$ can converge to the adjustable area $(-\varepsilon_l q_{T_s}, \varepsilon_h q_{T_s})$ nearly without overshoot in the preset time T_s. For the case of $e_1(0) = 0$, one can obtain the opposite property: $\dot{q}_l(t)\dot{q}_h(t) > 0$. $\tilde{e}_1$ meets the condition $-\varepsilon_l q(t) < \tilde{e}_1(t) < \varepsilon_h q(t)$, which is consistent with the common fixed-time convergence performance.

Next, the design of $o(t)$ needs to guarantee two conditions, i.e., $\tilde{e}_1(0) \in (-q_l(0), q_h(0))$ and $\tilde{e}_1 = e_1(t \geqslant T_D)$. Thereafter, the switching function $o(t)$ is constructed as

$$o(t) = \begin{cases} \frac{q_h(0) - q_l(0)}{2} \exp\left(1 - \frac{T_D}{T_D - t}\right), & 0 \leqslant t < T_D, \\ 0, & t \geqslant T_D. \end{cases} \tag{7}$$

Remark 5. Selecting sufficiently small parameter $\Delta \to 0$, for any $e_1(0)$ (consider $e_1(0) \nrightarrow \infty$ in the practical working environment), $\omega = r(0)e_1(0) \to 0$ always holds. Obviously, $-q_l(0) < \tilde{e}_1(0) = (q_h(0) - q_l(0))/2 + \omega < q_h(0)$ also holds and $\tilde{e}_1 = e_1(t \geqslant T_D)$, which removes the strict initial conditions of the tracking error given by traditional PCC methods and provides a solution to the practical problem that $e_1(0)$ cannot be guaranteed to be always within the constraint region.

The error transformation is designed as

$$z_1(t) = \tan\left(\frac{\pi \tilde{e}_1(t)}{q_h(t) + q_l(t)} - \frac{\pi(q_h(t) - q_l(t))}{2(q_h(t) + q_l(t))}\right). \tag{8}$$

By transformation, if $\tilde{e}_1(0) \in (-q_l(0), q_h(0))$ and $z_1(t) \in \mathcal{L}_\infty$ hold, then $\tilde{e}_1(t) \in (-q_l(t), q_h(t))$ holds. Note that $\tilde{e}_1(0) \in (-q_l(0), q_h(0))$ naturally holds. For $t \in [0, T_D)$, $r(t)$ and $o(t)$ are bounded by $(0, 1)$ and $(0, (q_h(0) - q_l(0))/2]$, respectively. Based on $\tilde{e}_1(t) = r(t)e_1(t) + o(t)$ and $\tilde{e}_1(t) \in (-q_l(t), q_h(t))$, one obtains $e_1(t) \in \mathcal{L}_\infty$ for $t \in [0, T_D)$. Further, from $\tilde{e}_1 = e_1(t \geqslant T_D)$, one obtains $e_1(t) \in (-q_l(t), q_h(t))$ for $t \in [T_D, +\infty)$. Keep $\varepsilon_h = \varepsilon_l$ as holding. If $\lim_{t\to+\infty} z_1(t) = 0$ holds, then $\lim_{t\to+\infty} e_1(t) = 2\arctan(0)\varepsilon_h q_{T_s}/\pi = 0$ holds.

3.2 Switching function matrix design

To prevent performance deterioration caused by an actuator fault in time, an effective solution is to design a mechanism for fault detection and automatic switching of the working mode. The working mode can be switched by changing the switching function matrix $Q(t) = \mathrm{diag}\{q_1(t) \dots q_M(t)\}$.

Definition 4. There exist W actuator fault patterns for M actuator channels, and the fth actuator fault pattern is defined as $\zeta_f := \{\zeta_{f1}, \zeta_{f2}, \dots, \zeta_{fl_f}\}$, where $\zeta_{f1}, \dots, \zeta_{fl_f} \in \{1, 2, \dots, M\}$ denote the channel serial numbers of the faulty actuator, and l_f is the sum of channels of the faulty actuator. Accordingly, its complement $\bar{\zeta}_f$ denotes the channel serial number set of a normal actuator.

Definition 5. For an actuator fault pattern ζ_f ($f \in \{1, 2, \dots, W\}$), define the undesired working mode set as $\Sigma_f := \{Q_{f1}, Q_{f2}, \dots, Q_{fL_f}\}$, where L_f is the sum of undesired working modes and the undesired working mode $Q_{fr} = \mathrm{diag}\{q_{fr1}\ q_{fr2} \dots\ q_{frM}\}$ ($r \in \{1,2, \dots, L_f\}$). If all $\beta_\sigma^j = 0$ ($j \in \{1, 2, \dots, M\}$), then $\Sigma_f = \emptyset$. Otherwise, Q_{fr} satisfies the following properties:

(i) $q_{frj} = \begin{cases} 1, & \text{if } \beta_\sigma^j = 1, \\ 0 \text{ or } 1, & \text{else;} \end{cases}$

(ii) $Q_{fr} \neq \mathbf{0}_{(M\times M)}$ where $\mathbf{0}_{(M\times M)}$ is a $M \times M$ zero matrix.

Definition 6. The set of overall working modes is given as $\bigcup := \{\bar{Q}_1, \bar{Q}_2, \dots, \bar{Q}_N\}$, where $\bar{Q}_i \neq \mathbf{0}_{(M,M)}$ ($i \in \{1, 2, \dots, N\}$) and $N = \sum_{S=1}^{M} C_M^S$.

Definition 7. With the fault pattern ζ_f ($f \in \{1, 2, \dots, W\}$), define the set of desired working mode candidates to be $\bar{\Sigma}_f := \bigcup -\Sigma_f$, where the desired working mode candidate $Q_{f\bar{r}} = \mathrm{diag}\{q_{f\bar{r}1}\ q_{f\bar{r}2} \dots q_{f\bar{r}M}\}$ ($\bar{r} \in \{1, 2, \dots, N-L_f\}$) and the compensation pattern of $Q_{f\bar{r}}$ is $J_{f\bar{r}} = \{j | q_{f\bar{r}j} = 0, j \in \{1, 2, \dots, M\}\}$ with $J_{f\bar{r}} \cup \bar{J}_{f\bar{r}} = \{1, 2, \dots, M\}$.

Remark 6. The PLOE actuator in multichannel environments may still maintain system performance, but the TLOE actuator can cause rapid performance deterioration or even system collapse. As shown in Definition 5, the working mode in which the control channel of the TLOE actuator is in the connected state is considered the undesired working mode to be switched. Moreover, $\bar{Q}_i \neq \mathbf{0}_{(M,M)}$ is a necessary prerequisite to ensure the overall controllability of the system, and $J_{f\bar{r}}$ represents the set of serial numbers of control channels in the disconnected state in mode $Q_{f\bar{r}}$ for subsequent analysis.

Taking the transformed error $z_1(t)$ as the detection signal, a learning-based switching mechanism for fault detection and automatic switching of the working mode is presented as follows. First, an update protocol of switching performance index ς is represented as $\dot{\varsigma} = k_\varsigma G(z_1(t))$ and $\varsigma(0) = 0$, where $k_\varsigma \in \mathbb{R}^+$ is a gain parameter and the switching function $G(z_1(t))$ is designed as

$$G(t) = \begin{cases} 0, & t = 0 \text{ or } -\bar{k}_1 h(t) < z_1(t) < \bar{k}_2 h(t), \\ \exp(-\bar{k}_3 \dot{z}_1^-)(-\bar{k}_1 h(t) - z_1(t))^{n_1}, & z_1(t) \leqslant -\bar{k}_1 h(t), \\ \exp(\bar{k}_4 \dot{z}_1^-)(-\bar{k}_2 h(t) + z_1(t))^{n_2}, & z_1(t) \geqslant \bar{k}_2 h(t), \end{cases} \tag{9}$$

where $\bar{k}_1$, $\bar{k}_2$, $\bar{k}_3$, and $\bar{k}_4 \in \mathbb{R}^+$; n_1 and $n_2 \geqslant 1$ are design parameters. $\dot{z}_1^- = (z_1(t) - z_1(t - t_k))/t_k$, where t_k is the minimum sampling interval. Additionally, construct $h(t)$ to be

$$h(t) = \begin{cases} \left(\frac{1}{t} - \frac{1}{T_h}\right)^{2\jmath} + \epsilon, & 0 < t < T_h, \\ \epsilon, & t \geqslant T_h, \end{cases} \tag{10}$$

where $\jmath \in \mathrm{N}^+$, T_h and $\epsilon \in \mathbb{R}^+$ are given design parameters.

Hereupon, design the switching function matrix to be $Q(t) := Q(\varsigma(t)) = \bar{Q}_\varpi \in \bigcup$ with $\varpi = \mathrm{mod}(\lfloor \varsigma \rfloor - 1, N) + 1$ in which ϖ denotes the switching mode index.

Remark 7. The working principle of the mechanism is as follows: if $Q(t)$ is set to a desired working mode, and the error z_1 is within the normal detection range, i.e., $z_1 \in (-\bar{k}_1 h, \bar{k}_2 h)$, then the switching parameters ς and ϖ remain unchanged, and $Q(t)$ cannot be switched; if $Q(t)$ is set to an inappropriate working mode, and z_1 is within the abnormal detection range, i.e., $z_1 \notin (-\bar{k}_1 h, \bar{k}_2 h)$, then according to (9) and (10), ς and ϖ, on the basis of the degree and trend of the signal exceeding the detection baseline, are driven to increase, and $Q(t)$ automatically switches until the desired working mode appears.

Remark 8. From the mapping relationship in error transformation (8), it is known that z_1 is more sensitive to faults than e_1 is, so the selection of z_1 as the detection signal is more reasonable and beneficial. Under the premise

of bounded stability of the system, considering the deferred constraints and the mapping relationship in (8), z_1 has no range limit in the initial period and then gradually converges to a specific bounded range. Thus, the funnel-like time-varying detection baselines $-\bar{k}_1 h$ and $\bar{k}_2 h$ are constructed to replace the horizontal detection baselines in the switching mechanism [36], thereby reducing the waste of frequent and unnecessary handover resources in the initial period.

3.3 Controller design

The coordinate transformations are introduced as

$$e_i = x_i - \alpha_{i-1},\ i = 2, \ldots, n, \tag{11}$$

where α_{i-1} is the virtual controllers. All α_{i-1} and common control protocol v_n are designed as

$$\alpha_1 = \mathcal{N}(\xi_1)\left(k_1\Gamma^{-1}z_1 + \frac{\hat{\Theta}_1 z_1 \Gamma r \mu_1^2}{\sqrt{(z_1\Gamma r\mu_1)^2 + \hbar^2}}\right);\ \alpha_i = \mathcal{N}(\xi_i)\left(k_i e_i + \frac{\hat{\Theta}_i e_i \mu_i^2}{\sqrt{(e_i\mu_i)^2 + \hbar^2}}\right), \tag{12}$$

$$v_n = \mathcal{N}(\xi_n)\left(k_n e_n + \frac{\hat{\Theta}_n e_n \mu_n^2}{\sqrt{(e_n\mu_n)^2 + \hbar^2}} + L\mathrm{sign}(e_n)\right),\ i = 2, \ldots, n-1, \tag{13}$$

where $k_j \in \mathbb{R}^+ (j = 1, \ldots, n)$ are design parameters. $L \in \mathbb{R}^+$ denotes a sufficiently large design parameter satisfying $L > \max_{k\in\Pi}\{\sum_{c=1}^{M} \bar{g}_{n,k}^c \bar{u}_k^c\}$. $\mathcal{N}(\xi_j)$ is the type-B Nussbaum odd function. $\Gamma = \pi(1+z_1^2)/(q_h+q_l)$, $\mu_1 = \|\varrho_1(\chi_1')\|+1$, and $\mu_i = |e_{i-1}^*| + \|\varrho_i(\chi_i')\| + 1$ $(i = 2, \ldots, n)$ are scalar functions with $e_1^* = \Gamma z_1$, $e_\kappa^* = e_\kappa$ $(\kappa = 2, \ldots, n-1)$, $\chi_1' = [x_1, y_r, r, o, q]^{\mathrm{T}}$, $\chi_2' = [\chi_1'^{\mathrm{T}}, x_2, \xi_1, \hbar, \hat{\Theta}_1]^{\mathrm{T}}$, and $\chi_l' = [\chi_{l-1}'^{\mathrm{T}}, x_l, \xi_{l-1}, \hat{\Theta}_{l-1}]^{\mathrm{T}}$ $(l = 3, \ldots, n)$. $\hbar \in \mathbb{R}^+$ meets $\int_0^t \hbar(\tau)d\tau \in (0, \bar{\hbar}]$ with $\bar{\hbar} < +\infty$.

The update laws of $\hat{\Theta}_l$ $(l = 1, \ldots, n)$ and ξ_l are designed as

$$\dot{\hat{\Theta}}_1 = \frac{\gamma_1(z_1\Gamma r\mu_1)^2}{\sqrt{(z_1\Gamma r\mu_1)^2 + \hbar^2}} - \gamma_1\hbar\hat{\Theta}_1,\ \dot{\hat{\Theta}}_i = \frac{\gamma_i(e_i\mu_i)^2}{\sqrt{(e_i\mu_i)^2 + \hbar^2}} - \gamma_i\hbar\hat{\Theta}_i,\ i = 2, \ldots, n, \tag{14}$$

$$\dot{\xi}_1 = \frac{\hat{\Theta}_1(z_1\Gamma r\mu_1)^2}{\sqrt{(z_1\Gamma r\mu_1)^2 + \hbar^2}} + k_1 r z_1^2,\ \dot{\xi}_j = \frac{\hat{\Theta}_j(e_i\mu_j)^2}{\sqrt{(e_j\mu_j)^2 + \hbar^2}} + k_j e_j^2,\ j = 2, \ldots, n-1, \tag{15}$$

$$\dot{\xi}_n = \frac{\hat{\Theta}_n(e_n\mu_n)^2}{\sqrt{(e_n\mu_n)^2 + \hbar^2}} + k_n e_n^2 + L|e_n|, \tag{16}$$

where $\gamma_l \in \mathrm{R}^+$ $(l = 1, \ldots, n)$ are design parameters.

3.4 Stability analysis

Theorem 1. For the switched nonlinear systems (1) with multichannel actuators and deferred constraints, under Assumptions 1–3, if the switching mechanism in Subsection 3.2, the control laws (12), (13), and update laws (14)–(16) hold, then all the closed-loop signals are SUUB under arbitrary switching. Additionally, tracking error $e_1(t)$ converges to the adjustable region $\{(t, e_1) \in \mathbb{R}_{\geqslant 0} \times \mathbb{R} | -\varepsilon_l q_{T_s} < e_1(t) < \varepsilon_h q_{T_s}\}$ in the preset time T_s and asymptotically reaches zero.

Proof. *Step 1.* Construct the Lyapunov function as $V_1 = z_1^2/2 + \tilde{\Theta}_1^2/(2\gamma_1)$, where $\tilde{\Theta}_1 = \Theta_1 - \hat{\Theta}_1$ is the estimate error with $\hat{\Theta}_1$ being the estimate of Θ_1. Using (1), (8), and (11), this function yields

$$\dot{V}_1 = z_1\Gamma r g_{1,k}(e_2 + \alpha_1) + z_1\Gamma r\left(f_{1,k}(x_1) - \dot{y}_r + r^{-1}(\dot{r}e_1 + o + \Omega\Gamma^{-1})\right) - \gamma_1^{-1}\tilde{\Theta}_1\dot{\hat{\Theta}}_1, \tag{17}$$

where $k \in \Pi$ and $\Omega = -((\dot{q}_h + \dot{q}_l)\arctan(z_1)/\pi + (\dot{q}_h - \dot{q}_l)/2)\Gamma$. $F_{1,k} = f_{1,k}(x_1) - \dot{y}_r + r^{-1}(\dot{r}e_1 + o + \Omega\Gamma^{-1})$ indicates an unknown and fussy function.

To address the design difficulties resulting from the unknown and fussy function $F_{1,k}$, the RBFNN in Subsection 2.3 is introduced, i.e., $F_{1,k} = \Xi_{1,k}^{\mathrm{T}}\varrho_1(\chi_1) + \delta_{1,k}(\chi_1)$ with $\chi_1 = [x_1, y_r, \dot{y}_r, r, \dot{r}, o, q, \dot{q}]^{\mathrm{T}}$. Define $\Theta_1 = \max_{k\in\Pi}\{\|\Xi_{1,k}\|, \bar{\delta}_{1,k}\}$. Using Lemma 1 and the applicable RBFNN characteristic in Lemma 3, one obtains the

simplified NN-based design process as follows:

$$\begin{aligned} z_1\Gamma r F_{1,k} &\leqslant |z_1|\Gamma r(\|\Xi_{1,k}\|\|\varrho_1(\chi_1')\| + \bar{\delta}_{1,k}) \\ &\leqslant \frac{\Theta_1(z_1\Gamma r\mu_1)^2}{\sqrt{(z_1\Gamma r\mu_1)^2+\hbar^2}} + \Theta_1\hbar. \end{aligned} \tag{18}$$

Inserting (12), (14), and (18) into (17) yields

$$\dot{V}_1 \leqslant z_1\Gamma r g_{1,k}e_2 + g_{1,k}\mathcal{N}(\xi_1)\dot{\xi}_1 + \dot{\xi}_1 - k_1 r z_1^2 + \hbar\left(\Theta_1 + \frac{\Theta_1^2}{4}\right). \tag{19}$$

Step i (2 $\leqslant i \leqslant n$). Construct the Lyapunov function as $V_i = V_{i-1} + e_i^2/2 + \tilde{\Theta}_i^2/(2\gamma_i)$, where $\tilde{\Theta}_i = \Theta_i - \hat{\Theta}_i$ is the estimate error with $\hat{\Theta}_i$ being the estimate of Θ_i.

Given step 1, it follows that $F_{i,k} = f_{i,k}(\bar{x}_i) - \sum_{l=1}^{i-1}\frac{\partial\alpha_i}{\partial x_l}(f_{l,k}(\bar{x}_l) + g_{l,k}x_{l+1}) - w_{i-1} = \Xi_{i,k}^{\mathrm{T}}\varrho_i(\chi_i) + \delta_{i,k}(\chi_i)$, where $w_{i-1} = \frac{\partial\alpha_{i-1}}{\partial y_r}\dot{y}_r + \frac{\partial\alpha_{i-1}}{\partial r}\dot{r} + \frac{\partial\alpha_{i-1}}{\partial o}\dot{o} + \frac{\partial\alpha_{i-1}}{\partial q}\dot{q} + \sum_{l=1}^{i-1}(\frac{\partial\alpha_{i-1}}{\partial\hat{\Theta}_l}\dot{\hat{\Theta}}_l + \frac{\partial\alpha_{i-1}}{\partial\xi_l}\dot{\xi}_l) + \frac{\partial\alpha_{i-1}}{\partial\hbar}\dot{\hbar}$, $\chi_2 = [\chi_1^{\mathrm{T}}, x_2, \xi_1, \dot{\xi}_1, \hbar, \dot{\hbar}, \hat{\Theta}_1, \dot{\hat{\Theta}}_1, \dot{o}]^{\mathrm{T}}$, and $\chi_{i'} = [\chi_{i'-1}^{\mathrm{T}}, x_{i'}, \xi_{i'-1}, \dot{\xi}_{i'-1}, \hat{\Theta}_{i'-1}, \dot{\hat{\Theta}}_{i'-1}]^{\mathrm{T}}$ $(3 \leqslant i' \leqslant n)$.

Following the simplified NN-based design process, one has

$$\dot{V}_n \leqslant -k_1 r z_1^2 - \sum_{m=2}^{n} k_m e_m^2 + \sum_{j=1}^{n-1}(g_{j,k}\mathcal{N}(\xi_j)\,\dot{\xi}_j + \dot{\xi}_j) + \dot{\xi}_n + e_n g_{n,k}u_k - \max_{k\in\Pi}\left\{|e_n|\sum_{c=1}^{M}\bar{g}_{n,k}^c\bar{u}_k^c\right\} + \bar{\Theta}, \tag{20}$$

where $\bar{\Theta} = \sum_{j=1}^{n}\hbar(\Theta_j + \frac{\Theta_j^2}{4})$ and $\Theta_i = \max_{k\in\Pi}\{\|\Xi_{i,k}\|, \bar{g}_{i-1,k}, \bar{\delta}_{i,k}\}$.

Then, $e_n g_{n,k}u_k$ is analyzed in two cases of $Q(t)$.

(i) $Q(t)$ is set to the appropriate working mode $Q(t) = Q_{f\bar{r}} \in \bar{\Sigma}_f$ with $\zeta_f \subset J_{f\bar{r}}$. Thereafter, it yields

$$\begin{aligned} e_n g_{n,k}u_k &= e_n\sum_{c\in\zeta_f} g_{n,k}^c\vartheta_k^c(0,t) + e_n\sum_{c\in\bar{J}_{f\bar{r}}} g_{n,k}^c v_k^c \\ &\leqslant G_{n,k}^{f_{\bar{r}}}(t)\mathcal{N}(\xi_n)\dot{\xi}_n + \max_{k\in\Pi}\left\{|e_n|\sum_{c=1}^{M}\bar{g}_{n,k}^c\bar{u}_k^c\right\}, \end{aligned} \tag{21}$$

where $G_{n,k}^{f_{\bar{r}}}(t) = \sum_{c\in\bar{J}_{f\bar{r}}} g_{n,k}^c$ with $G_{n,k}^{f_{\bar{r}}}(t) \in (0, \sum_{c=1}^{M}\bar{g}_{n,k}^c)$.

(ii) $Q(t)$ is set to the general working mode $Q(t) = \bar{Q}_\varpi \in \bigcup$ with $\zeta_f \not\subset J_\varpi$. Thereafter, it yields

$$\begin{aligned} e_n g_{n,k}u_k &\leqslant \sum_{c\in\bar{\zeta}_f\cap\bar{J}_\varpi} g_{n,k}^c\mathcal{N}(\xi_n)\dot{\xi}_n + e_n\sum_{c\in\zeta_f\cap\bar{J}_\varpi\cap\bar{\Phi}_\varpi} g_{n,k}^c\rho_k^c v_k^c + |e_n|\left(\sum_{c\in\zeta_f\cap J_\varpi}\bar{g}_{n,k}^c\bar{u}_k^c + \sum_{c\in\zeta_f\cap\bar{J}_\varpi\cap\Phi_\varpi}\bar{g}_{n,k}^c\bar{u}_k^c\right) \\ &\leqslant G_{n,k}^{\varpi}(t)\mathcal{N}(\xi_n)\dot{\xi}_n + \max_{k\in\Pi}\left\{|e_n|\sum_{c=1}^{M}\bar{g}_{n,k}^c\bar{u}_k^c\right\}, \end{aligned} \tag{22}$$

where $G_{n,k}^{\varpi}(t) = \sum_{c\in\bar{\zeta}_f\cap\bar{J}_\varpi} g_{n,k}^c + \sum_{c\in\zeta_f\cap\bar{J}_\varpi\cap\bar{\Phi}_\varpi} g_{n,k}^c\rho_k^c$ with $G_{n,k}^{\varpi}(t) \in (0, \sum_{c=1}^{M}\bar{g}_{n,k}^c)$.

Further, Eq. (20) is rewritten as

$$\dot{V}_n \leqslant -k_1 r z_1^2 - \sum_{m=2}^{n} k_m e_m^2 + \sum_{j=1}^{n}\left(g_{j,k}\mathcal{N}(\xi_j)\dot{\xi}_j + \dot{\xi}_j\right) + \sum_{j=1}^{n}\hbar\left(\Theta_j + \frac{\Theta_j^2}{4}\right), \tag{23}$$

where

$$g_{n,k} = \begin{cases} G_{n,k}^{f_{\bar{r}}}(t),\ Q(t) = Q_{f_{\bar{r}}} \in \bar{\Sigma}_f \text{ with } \zeta_f \subset J_{f\bar{r}}, \\ G_{n,k}^{\varpi}(t),\ Q(t) = \bar{Q}_\varpi \in \bigcup \text{ with } \zeta_f \not\subset J_\varpi. \end{cases}$$

Integration of (23) yields

$$V_n(t)+\int_0^t k_1 r z_1^2 d\tau+\sum_{m=2}^{n}\int_0^t k_m e_m^2 d\tau\sum_{j=1}^{n}\int_0^t (g_{j,k}\mathcal{N}(\xi_j)+1)\dot{\xi}_j d\tau+\sum_{j=1}^{n}\left(\Theta_j+\frac{\Theta_j^2}{4}\right)\int_0^t \hbar(\tau)d\tau. \tag{24}$$

Relying on the integral property of $\hbar(t)$ and Lemma 2, it holds that ξ_j, V_n, and $\hat{\Theta}_j \in \mathcal{L}_\infty$. z_1 and $e_m \in \mathcal{L}_\infty \cap \mathcal{L}_2$. By transformation (8), (11), and control laws (12), (13), one obtains α_i $(i=1,\ldots,n-1)$, x_j, v_n, $\dot{z}_1$, and $\dot{e}_m \in \mathcal{L}_\infty$. Additionally, it yields $e_1(t) \in \mathcal{L}_\infty$ for $t \in [0,\, T_D)$ and $e_1(t) \in (-q_l(t), q_h(t))$ for $t \in [T_D, +\infty)$. Thus, all the closed-loop signals are SUUB under arbitrary switching, and $e_1(t)$ converges to $\{(t,e_1) \in \mathbb{R}_{\geqslant 0}\times\mathbb{R} | -\varepsilon_l q_{T_s} < e_1(t) < \varepsilon_h q_{T_s}\}$ in T_s. By the Barbalat's lemma, $\lim_{t\to+\infty} z_1(t)=0$ holds from $z_1 \in \mathcal{L}_\infty \cap \mathcal{L}_2$ and $\dot{z}_1 \in \mathcal{L}_\infty$. Then, $\lim_{t\to+\infty} e_1(t)=0$ holds with $\varepsilon_h=\varepsilon_l$.

Remark 9. In the given control design procedure, the core or actual activation signals χ_i' $(i=1,\ldots,n)$ without derivative variables (e.g., $\dot{y}_r$ and $\dot{\xi}_i$) are introduced to replace the initial activation signals χ_i, which not only removes the assumption of *a priori* knowledge of the high-order derivatives of y_r being known but also averts an "explosion of complexity" due to repeated calculation of derivatives in virtual controllers without using a dynamic surface or command filtering technique.

4 Simulation results

In this section, two simulation examples and a comprehensive analysis are performed to refine the research architecture and show the superiority of the proposed control method.

Example 1. Consider the typical switched nonlinear systems with multichannel actuators, where $\sigma:[0,\infty)\to \Pi=\{1,2\}$, $g_{1,1}(x_1,t)=1+0.4\sin(x_1)+0.1\sin^4(t)$, $f_{1,1}(x_1)=\cos^3(x_1)$, $g_{2,1}^c(t)=1+0.5\sin(t)$, $f_{2,1}(\bar{x}_2)=-x_1-\sin^2(x_1)-\sin(x_2)$, $g_{1,2}(x_1,t)=1.1+0.5\sin(x_1)+0.1\cos^4(t)$, $f_{1,2}(x_1)=1.2\cos^3(x_1)$, $g_{2,2}^c(t)=0.5+0.1\cos(t)$ and $f_{2,2}(\bar{x}_2)=-1.2x_1-2\sin^2(x_1)-x_1^2\sin(x_2)$. To verify the effectiveness of the proposed fault-tolerant controller, the following set of corresponding overall working modes $\bigcup$ and specific three-channel actuator fault pattern $\zeta_6=\{2,3\}$ are given.

It is assumed that the actuator of the second channel encounters PLOE with $u_\sigma^2=\vartheta(q_2v_\sigma^2,t)=0.7q_2v_\sigma^2$, $t\geqslant 1$ s, and the actuator of the third channel suffers from TLOE with $u_\sigma^3=\vartheta(q_3v_\sigma^3,t)=1$, $t\geqslant 8$ s. $\bigcup$ is defined as $\bigcup:=\{\bar{Q}_1,\bar{Q}_2,\ldots,\bar{Q}_7\}=\{\text{diag}\{0\ 0\ 1\},\ \text{diag}\{0\ 1\ 0\},\ \text{diag}\{0\ 1\ 1\},\ \text{diag}\{1\ 0\ 0\},\ \text{diag}\{1\ 0\ 1\},\ \text{diag}\{1\ 1\ 0\},\ \text{diag}\{1\ 1\ 1\}\}$. Further, the desired working mode candidates are $\bar{Q}_2$, $\bar{Q}_4$, and $\bar{Q}_6$.

Assign the reference signal as $y_r=-2.5\sin(0.6t)+0.2$, and the initial conditions are $x(0)=[-1,0]^{\mathrm{T}}$, $\hat{\Theta}_1(0)=\hat{\Theta}_2(0)=\xi_1(0)=\xi_2(0)=\varsigma(0)=0$. Choose the type-$B$ Nussbaum function as $\mathcal{N}(\xi)=\exp(\xi^2)\cos(0.5\pi\xi)\xi^3$. Configure the performance parameters as $q_0=0.6$, $q_{T_s}=0.1$, $p=2$, $\nu=1$, $\varepsilon_h=\varepsilon_l=0.8$, $T_D=0.4$, and $\Delta=0.01$. The relevant structure of the RBFNN is shown below: $\varrho_1(\chi_1')$ contains five hidden nodes, and the centers are evenly distributed in the field $[-2,2]^5$ with the width 2; $\varrho_2(\chi_2')$ contains five hidden nodes, and the centers are evenly distributed in the field $[-2,2]^9$ with the width 2. The remaining parameters are set as $k_1=k_2=\bar{k}_1=\bar{k}_2=n_1=n_2=\gamma_1=\gamma_2=L=1$, $T_h=2$, $\epsilon=0.15$, $\bar{k}_3=\bar{k}_4=0.01$, $k_\varsigma=6000$, and $\jmath=1$. The integrable function is $\hbar=10\exp(-t)$.

The synthetic simulation results are provided in Figures 2–5. Figure 2 shows that the output signal y rapidly enters the user-defined reference range and sustains excellent tracking performance. Figure 3 shows that tracking errors e_1 with different deferred constraint times T_D converge to the specified area $(-\varepsilon_l q_{T_s}, \varepsilon_h q_{T_s})$ nearly without overshoot in the preset time T_s. Figure 4 shows that when the transformed error z_1 undergoes faults that exceed the detection baseline, the designed mechanism automatically switches the working mode to ensure that z_1 converges to the plateau again, thus avoiding fault-caused system collapse. Figure 5 displays the switching performance index ς and mode index ϖ. u_σ^3 suffers from TLOE at $t=8$ s, which makes $\bar{Q}_1$ become an undesired working mode, resulting in z_1 rapidly exceeding the detection baseline. Therefore, the indices ς and ϖ keep growing until ϖ reaches 2, and $\bar{Q}_1$ automatically switches to the desired working mode $\bar{Q}_2$. Then, z_1 returns to the plateau, the indices stop growing, and the working mode remains at $\bar{Q}_2$.

Example 2. Consider the mass-spring-damper system with controller switching in $[1,41]$. Suppose that there

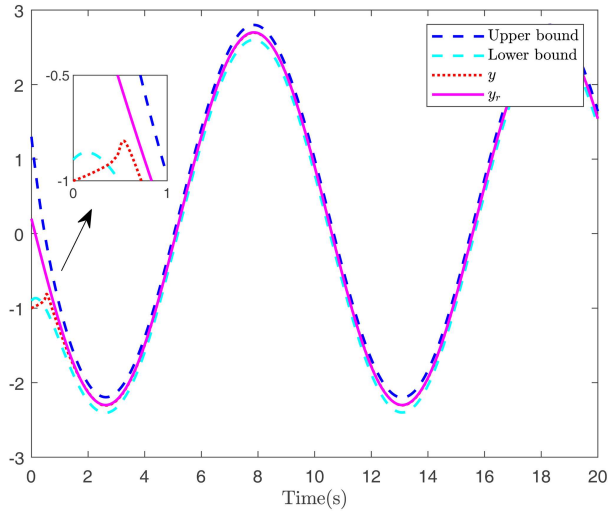

Figure 2 (Color online) Rendering of the tracking situation.

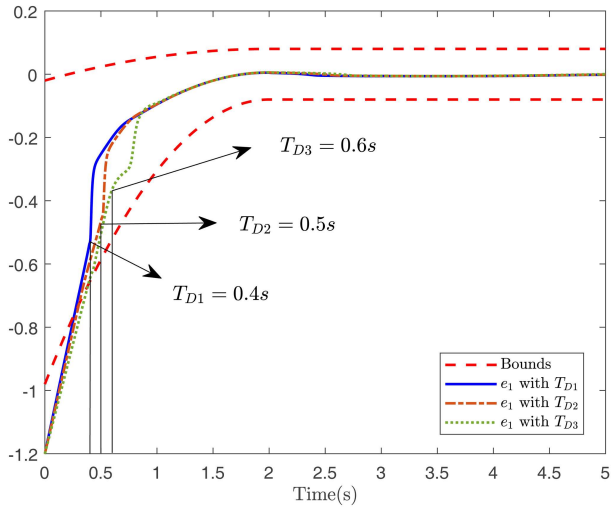

Figure 3 (Color online) Error constraint rendering with different deferred constraint times.

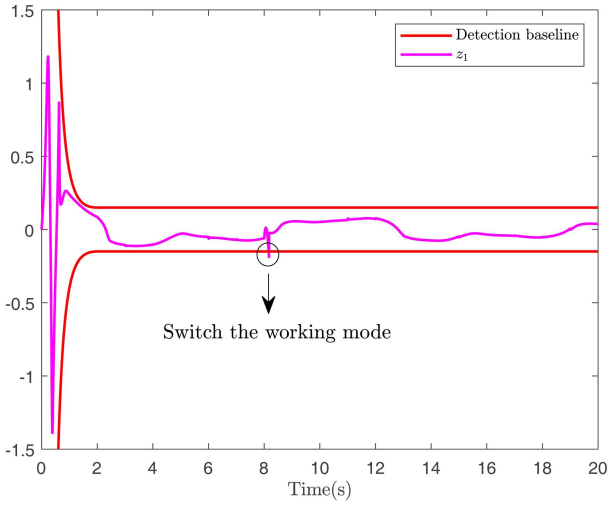

Figure 4 (Color online) Rendering of the transformed error undergoing faults.

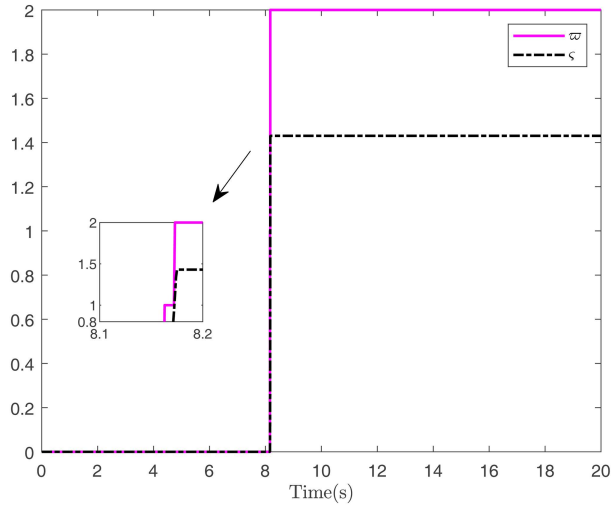

Figure 5 (Color online) Rendering of the switching performance index and the mode index.

exists candidate controllers $\bar{u}_\sigma = -f_\sigma(x_1) + B_\sigma^{\mathrm{T}} u_\sigma$ with $f_\sigma(0) = 0$. In the light of [41], the system is written as

$$\begin{cases} \dot{x}_1 = x_2, \\ \dot{x}_2 = \dfrac{1}{J} B_\sigma^{\mathrm{T}} u_\sigma - \dfrac{\omega_1}{J} x_1 - \dfrac{\omega_1 \omega_3^2}{J} x_1^3 - \dfrac{\omega_2}{J} x_2 - \dfrac{1}{J} f_\sigma(x_1), \\ y = x_1, \end{cases} \tag{25}$$

where $\sigma : [0, \infty) \to \Pi = \{1, 2\}$, $B_\sigma = [b_\sigma^1, b_\sigma^2, b_\sigma^3]^{\mathrm{T}}$, $u_\sigma = [u_\sigma^1, u_\sigma^2, u_\sigma^3]^{\mathrm{T}}$, $b_1^1 = b_1^2 = b_1^3 = 1/4$, $b_2^1 = b_2^2 = b_2^3 = 1/6$, $f_1(x_1) = -\omega_1 \omega_3^5 x_1^2 \cos(x_1^3)$, and $f_2(x_1) = -2\omega_1 \omega_3^2 x_1^3 \sin(x_1)$. Concretely, $\bar{u}_\sigma$, x_1, x_2, and y denote the external driving force, displacement, velocity, and measured displacement, respectively. The physical parameters of the systems J, ω_1, ω_2, and ω_3 indicate mass, linear elastic coefficient, viscous friction coefficient, and nonlinear elastic coefficient, respectively. Without loss of generality, it is considered that x_2 can be measured by a speed sensor, and the parameters J and ω_i $(i = 1, 2, 3)$ meet the constraint conditions $4 \leqslant 1/J \leqslant 4.1$ and $0 < \omega_i \leqslant 1/4$ in [41]. Thus, fit the system parameters as $J = 1/4$ kg and $\omega_1 = \omega_2 = \omega_3 = 1/4$. In addition to the same parameter configuration as in Example 1, select the reference signal as $y_r = 2.5 \sin(0.6t) - 0.2$. The initial state vector is $x(0) = [1, 0]^{\mathrm{T}}$. Let $k_1 = 0.6$ and $k_\varsigma = 3000$. The assumed three channel fault case is as follows: the actuator of the third channel

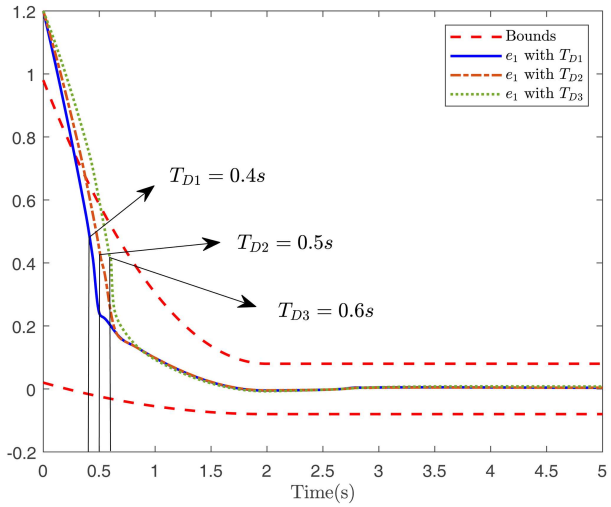

Figure 6 (Color online) Error constraint rendering with different deferred constraint times.

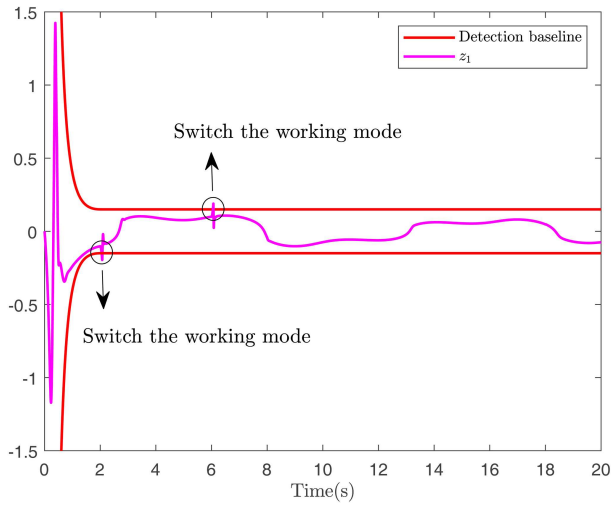

Figure 7 (Color online) Rendering of the transformed error undergoing faults.

encounters TLOE with $u_\sigma^3 = \vartheta(q_3 v_\sigma^3, t) = -1,\ t \geqslant 2$ s; and the actuator of the second channel suffers from TLOE with $u_\sigma^2 = \vartheta(q_2 v_\sigma^2, t) = 0,\ t \geqslant 6$ s. Obviously, the desired working mode candidate is $\bar{Q}_4$. Major simulation results for the system (25) are shown in Figures 6 and 7.

Comprehensive analysis. To better demonstrate the robustness of the proposed method, more multichannel actuator operation cases are discussed and analyzed, which are listed as follows. (1) The multichannel actuators operate normally, i.e., FF. (2) The actuator of the second channel encounters PLOE with $u_\sigma^2 = \vartheta(q_2 v_\sigma^2,\ t) = 0.3 q_2 v_\sigma^2,\ t \geqslant 2$ s, and the actuator of the third channel suffers from TLOE with $u_\sigma^3 = \vartheta(q_3 v_\sigma^3, t) = 0,\ t \geqslant 14$ s. (3) The actuator of the first channel encounters PLOE with $u_\sigma^1 = \vartheta(q_1 v_\sigma^2, t) = 0.9 q_1 v_\sigma^1,\ t \geqslant 5$ s, the actuator of the second channel encounters TLOE with $u_\sigma^2 = \vartheta(q_2 v_\sigma^2, t) = 1,\ t \geqslant 9$ s, and the actuator of the third channel suffers from TLOE with $u_\sigma^3 = \vartheta(q_3 v_\sigma^3, t) = 5,\ t \geqslant 2$ s. (4) The actuators of the first and third channels simultaneously encounter TLOE with $u_\sigma^1 = u_\sigma^3 = 0,\ t \geqslant 4$ s. The evolution of the transformed error in Figure 8 shows that under four general actuator operation cases, the error remains stable within the normal range of detection continuously or via automatic fault accommodation. Thus, the proposed FTC method provides good robustness. Then, two recent PCC methods are chosen to compare tracking performance with the proposed method (all analogous performance parameters are consistent). The PCC method 1 in [24] achieves the preset time convergence performance without initial conditions, and the PCC method 2 in [23] achieves the tracking performance without obvious overshoot. The index $Int(e_1, T) = \int_0^T \tau |e_1(\tau)| d\tau$ is used to quantitatively appraise the overall tracking performance. The index values of the three methods are $Int(e_1, 5) = 0.0835$ in method 1, $Int(e_1, 5) = 0.2512$ in method 2 and $Int(e_1, 5) = 0.0486$ in the proposed method, respectively. Obviously, the index value of the proposed method has the smallest index value. From Figure 9, compared with the other two methods, the proposed method realizes rapid error convergence within two seconds without obvious overshoot. Additionally, the corresponding steady-state error level is more stable and lower. Combined with the index values and Figure 9, the proposed method can clearly improve the overall tracking performance. Moreover, to underscore the superiority of the proposed mechanism, a comparative analysis of switching indices between the comparable FTC method in [36] and the proposed method is conducted in two fault cases. Case 1 is selected as the case in Example 2. Case 2 is below: the actuator of the first channel encounters PLOE with $u_\sigma^1 = \vartheta(q_1 v_\sigma^1, t) = 0.1 q_1 v_\sigma^1,\ t \geqslant 1$ s; the actuator of the third channel suffers from TLOE with $u_\sigma^3 = \vartheta(q_3 v_\sigma^3, t) = 0,\ t \geqslant 6$ s. From Figures 10 and 11, the proposed method reflects fewer and more efficient handover actions and, in particular, prevents the frequent mode switching behavior of the comparable FTC method in the first two seconds. Thus, the proposed method can reduce or even avoid the waste of unnecessary handover resources in the initial period, and further optimize the fault detection and accommodation behavior.

Remark 10. The parameter setting for the experimental setup mainly adheres to four aspects: the conditions of design parameters, the experience of parameter adjustment, the physical constraints of system parameters, and the performance influence. First, all the design parameters must meet the given design conditions. Second, certain experiences contribute to the rapid selection of reasonable parameters. Third, for the practical system model, the system parameters must meet the physical constraints. Thus, the selection of parameters in model (25) is consistent with that in [41]. Finally, parameters should be selected on the basis of performance. Small T_s ensures

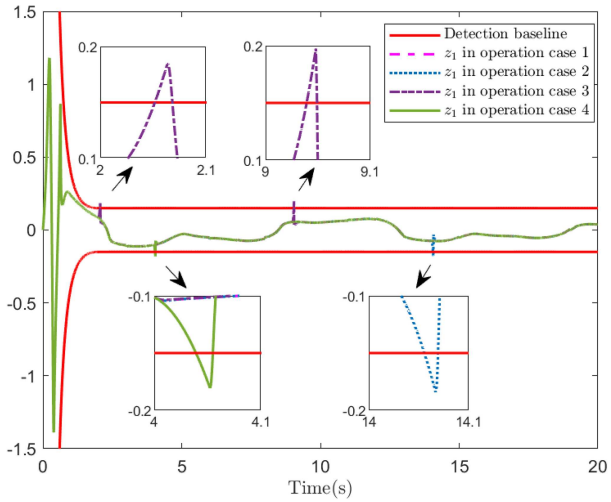

Figure 8 (Color online) Rendering of the transformed error undergoing operation cases.

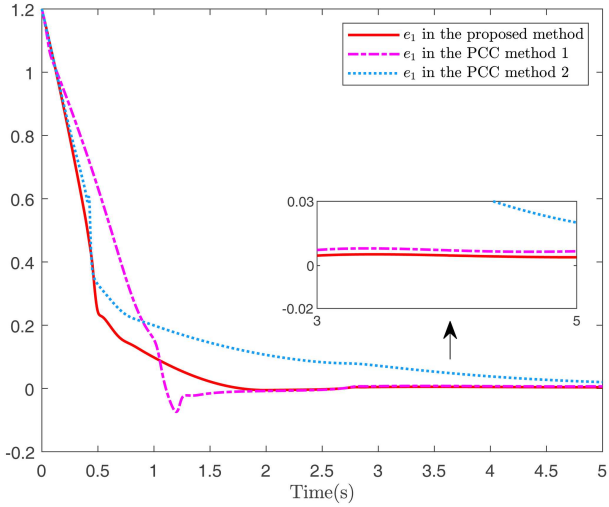

Figure 9 (Color online) Rendering of the tracking error comparison among three methods.

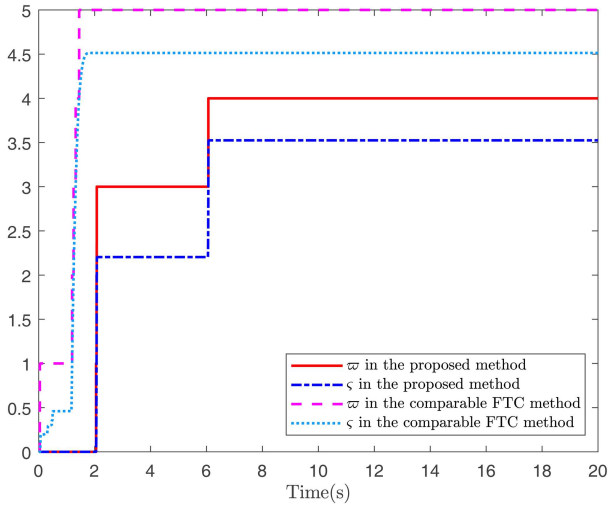

Figure 10 (Color online) Rendering of the index comparison between two methods in case 1.

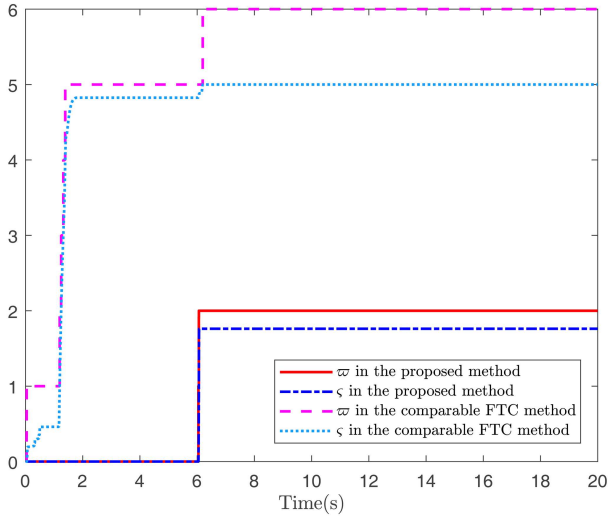

Figure 11 (Color online) Rendering of the index comparison between two methods in case 2.

fast convergence performance. Small q_{T_s}, ε_l and ε_h maintain high tracking accuracy. T_D, which is limited to a small and reasonable range, ensures that the initial dynamic performance does not become poor.

5 Conclusion

An improved adaptive FTC design scheme was presented for a switched nonlinear system with multichannel actuators and deferred constraints. The restrictions on the monotonicity of Nussbaum's arguments were removed by the proposed Lemma 2. Synthetic stability analysis and simulation results proved that all the closed-loop signals are SUUB under arbitrary switching, and an improved FTC controller can drive the tracking error with deferred constraints to converge to a specified region without obvious overshoot in a preset time. Moreover, the fault detection and accommodation behavior were optimized under the proposed mechanism compared with the analogous mechanism. Considering network communication, we intend to extend this control idea to switched heterogeneous systems in a future study.

Acknowledgements This work was supported by National Natural Science Foundation of China (Grant No. 62373137).

References

1 Shu F, Zhai J. Event-triggered prescribed-time tracking control for nonlinear systems with asynchronous switching. IEEE Trans Circuits Syst I, 2023, 70: 4159–4168
2 Wu L B, Park J H, Xie X P, et al. Adaptive fuzzy tracking control for a class of uncertain switched nonlinear systems with full-state constraints and input saturations. IEEE Trans Cybern, 2021, 51: 6054–6065
3 Li S, Ahn C K, Guo J, et al. Neural-network approximation-based adaptive periodic event-triggered output-feedback control of switched nonlinear systems. IEEE Trans Cybern, 2021, 51: 4011–4020
4 Song X, Man J, Song S, et al. Finite-time fault estimation and tolerant control for nonlinear interconnected distributed parameter systems with Markovian switching channels. IEEE Trans Circuits Syst I, 2022, 69: 1347–1359
5 Qian W, Lu D, Guo S, et al. Distributed state estimation for mixed delays system over sensor networks with multichannel random attacks and Markov switching topology. IEEE Trans Neural Netw Learn Syst, 2024, 35: 8623–8637
6 Zhou Q, Li H, Wu C, et al. Adaptive fuzzy control of nonlinear systems with unmodeled dynamics and input saturation using small-gain approach. IEEE Trans Syst Man Cybern Syst, 2017, 47: 1979–1989
7 Pan Y, Du P, Xue H, et al. Singularity-free fixed-time fuzzy control for robotic systems with user-defined performance. IEEE Trans Fuzzy Syst, 2021, 29: 2388–2398
8 Li H, Bai L, Zhou Q, et al. Adaptive fuzzy control of stochastic nonstrict-feedback nonlinear systems with input saturation. IEEE Trans Syst Man Cybern Syst, 2017, 47: 2185–2197
9 Long L, Zhao J. Adaptive output-feedback neural control of switched uncertain nonlinear systems with average dwell time. IEEE Trans Neural Netw Learn Syst, 2015, 26: 1350–1362
10 Qian W, Xing W, Fei S. State estimation for neural networks with general activation function and mixed time-varying delays. IEEE Trans Neural Netw Learn Syst, 2021, 32: 3909–3918
11 Zhou B, Huang X, Song Y, et al. Asymptotic tracking control for uncertain mimo nonlinear systems with guaranteed performance and enhanced controllability. IEEE Trans Automat Contr, 2024, 69: 4005–4012
12 Wang X, Zhou Y, Luo B, et al. Event-triggered neuro-adaptive fixed-time control for nonlinear switched and constrained systems: an initial condition-independent method. IEEE Trans Circuits Syst I, 2024, 71: 2229–2239
13 Liu Y J, Tong S. Barrier Lyapunov functions for Nussbaum gain adaptive control of full state constrained nonlinear systems. Automatica, 2017, 76: 143–152
14 Chen W, Li X, Ren W, et al. Adaptive consensus of multi-agent systems with unknown identical control directions based on a novel Nussbaum-type function. IEEE Trans Automat Contr, 2014, 59: 1887–1892
15 Chen Z. Nussbaum functions in adaptive control with time-varying unknown control coefficients. Automatica, 2019, 102: 72–79
16 Hua C C, Li H, Li K, et al. Adaptive prescribed-time stabilization of uncertain nonlinear systems with unknown control directions. IEEE Trans Automat Contr, 2024, 69: 3968–3974
17 Zhao K, Song Y, Ma T, et al. Prescribed performance control of uncertain Euler-Lagrange systems subject to full-state constraints. IEEE Trans Neural Netw Learn Syst, 2018, 29: 3478–3489
18 Yuan R, An Z C, Shao S Y, et al. Dynamic event-triggered fault-tolerant cooperative resilient tracking control with prescribed performance for UAVs. Sci China Inf Sci, 2024, 67: 180205
19 Ji R, Li D, Ma J, et al. Saturation-tolerant prescribed control of mimo systems with unknown control directions. IEEE Trans Fuzzy Syst, 2022, 30: 5116–5127
20 Wang F, Long L. Switched-observer-based event-triggered adaptive fuzzy funnel control for switched nonlinear systems. IEEE Trans Fuzzy Syst, 2022, 30: 1773–1787
21 Yao Y, Tan J, Yao Y, et al. Prescribed-time prescribed performance control for stochastic nonlinear input-delay systems with arbitrary bounded initial error. Neurocomputing, 2024, 571: 127200
22 Yue X, Zhang H, Sun J, et al. A simplified fuzzy wavelet neural control for nonlinear systems with quantized inputs and deferred constraints. IEEE Trans Fuzzy Syst, 2024, 32: 1504–1514
23 Ji R, Li D, Ge S S, et al. Tunnel prescribed control of nonlinear systems with unknown control directions. IEEE Trans Neural Netw Learn Syst, 2023, 36: 1383–1395
24 Liu P M, Guo X G, Wang J L, et al. Preset-time and preset-accuracy human-in-the-loop cluster consensus control for MASs under stochastic actuation attacks. IEEE Trans Automat Contr, 2024, 69: 1675–1688
25 Zhang T L, Deng F Q, Sun Y, et al. Fault estimation and fault-tolerant control for linear discrete time-varying stochastic systems. Sci China Inf Sci, 2021, 64: 200201
26 Zhang C C, Yang H, Jiang B. Fault-tolerant flocking control against multiple malicious agents under geometric configuration containment. Sci China Inf Sci, 2024, 67: 202204
27 Sui S, Tong S. FTC design for switched fractional-order nonlinear systems: an application in a permanent magnet synchronous motor system. IEEE Trans Cybern, 2023, 53: 2506–2515
28 Liu M, Liu Q H, Zhang L X, et al. Adaptive dynamic programming-based fault-tolerant attitude control for flexible spacecraft with limited wireless resources. Sci China Inf Sci, 2023, 66: 202201
29 Shen Q, Jiang B, Cocquempot V. Adaptive fuzzy observer-based active fault-tolerant dynamic surface control for a class of nonlinear systems with actuator faults. IEEE Trans Fuzzy Syst, 2014, 22: 338–349
30 Ferrari R M G, Parisini T, Polycarpou M M. Distributed fault detection and isolation of large-scale discrete-time nonlinear systems: an adaptive approximation approach. IEEE Trans Automat Contr, 2012, 57: 275–290
31 Iqbal R, Maniak T, Doctor F, et al. Fault detection and isolation in industrial processes using deep learning approaches. IEEE Trans Ind Inf, 2019, 15: 3077–3084
32 Qian W, Wu Y, Yang J. Event-driven reduced-order fault detection filter design for nonlinear systems with complex communication channel. IEEE Trans Fuzzy Syst, 2024, 32: 281–293
33 Steffen T, Schiller F, Blum M, et al. Analysing the reliability of actuation elements in series and parallel configurations for high-redundancy actuation. Int J Syst Sci, 2013, 44: 1504–1521
34 Ouyang H, Lin Y. Adaptive fault-tolerant control for actuator failures: A switching strategy. Automatica, 2017, 81: 87–95
35 Yang Q, Ge S S, Sun Y. Adaptive actuator fault tolerant control for uncertain nonlinear systems with multiple actuators. Automatica, 2015, 60: 92–99
36 Ruan Z, Yang Q, Ge S S, et al. Adaptive fuzzy fault tolerant control of uncertain MIMO nonlinear systems with output constraints and unknown control directions. IEEE Trans Fuzzy Syst, 2022, 30: 1224–1238
37 Song Y, Wang Y, Wen C. Adaptive fault-tolerant pi tracking control with guaranteed transient and steady-state performance. IEEE Trans Automat Contr, 2017, 62: 481–487
38 Bechlioulis C P, Rovithakis G A. Adaptive control with guaranteed transient and steady state tracking error bounds for strict feedback systems. Automatica, 2009, 45: 532–538
39 Li Y, Wu L, Hu Y. Fault-tolerant control for nonlinear switched systems with unknown control coefficients and full-state constraints. Inf Sci, 2022, 582: 750–766
40 Li Y X. Command filter adaptive asymptotic tracking of uncertain nonlinear systems with time-varying parameters and disturbances. IEEE Trans Automat Contr, 2022, 67: 2973–2980

41 Long L, Zhao J. Output-feedback stabilisation for a class of switched nonlinear systems with unknown control coefficients. Int J Control, 2013, 86: 386–395

Appendix A Proof of Lemma 2

For continuous differentiable functions $\xi_i(t)$ $(i = 1, 2, \ldots, n)$, there exist continuous time intervals, i.e., $[0, T_1)$, …, $[T_k, T_{k+1})$ $(k = 1, 2, \ldots, +\infty)$, as shown in Figure A1, where •, △, and ∘ denote inflection points of $\xi_1(t)$, $\xi_2(t)$, and $\xi_3(t)$ $(n = 3)$, respectively, so that all $\xi_i(t)$ possess monotonicity in each interval. Thereafter, the boundedness of $\xi_i(t)$ is proved in three steps by mathematical induction.

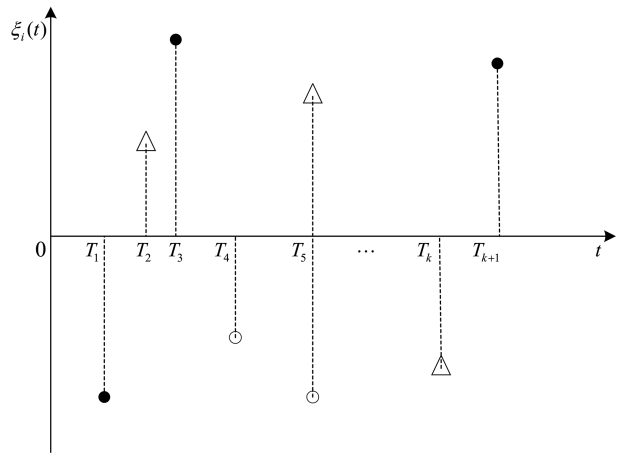

Figure A1 Rendering of inflection points of $\xi_i(t)$ $(i = 1, 2, 3)$.

Step 1. Three cases of $\xi_i(t)$ are discussed for $t \in [0, T_1)$ as follows.

Case I. All $\xi_i(t) \in \mathcal{L}_\infty$ hold. It is not difficult to show that $\lim_{t\to T_1^-} \xi_i(t) = \xi_i(T_1^-) \in \mathcal{L}_\infty$.

Case II. $\xi_1(t), \ldots, \xi_j(t) \notin \mathcal{L}_\infty$ and $\xi_{j+1}(t), \ldots, \xi_n(t) \in \mathcal{L}_\infty (0 < j < n)$ hold. For one condition $g_i(t) > 0$, there exists the set $l = \{l_1, l_2, \ldots\}$ with $l_1 < l_2 < \ldots$ and $l_1 \to +\infty$, which satisfies the following two properties.

(i) Define $\xi_\eta(t) := \max\{|\xi_1(t)|, \ldots, |\xi_j(t)|\}$ with $t \in [0, T_1)$. Considering the monotonicity of $\xi_i(t)$, there exists the set $t^* = \{t_1, t_2, \ldots\}$ with $t_1 < t_2 < \ldots$ and $t^* \subset [0, T_1)$, so that $\xi_\eta(\cdot) : t^* \to l$ holds and the relationship between two sets is one-to-one mapping.

(ii) For any $l_p \in l$, it holds that $\lim_{l_p\to+\infty} \frac{\int_0^{l_p} N^-(\tau)d\tau}{l_p} = +\infty$ and $\lim_{l_p\to+\infty} \frac{\int_0^{l_p} N^-(\tau)d\tau}{\int_0^{l_p} N^+(\tau)d\tau} = +\infty$.

Base on the integral property of the Nussbaum odd function $N(\xi)$, for any $t_p \in t^*$, it yields

$$V(t_p) \leqslant \int_0^{\xi_\eta(t_p)} g_\eta(\tau)\left(N^+(\xi_\eta(\tau)) - N^-(\xi_\eta(\tau))\right) d\xi_\eta(\tau) + \sum_{i=1, i\neq\eta}^{j} \int_0^{|\xi_i(t_p)|} g_i(\tau)N(\xi_i(\tau))d\xi_i(\tau)$$
$$+ \sum_{i=1}^{j} \int_0^{|\xi_i(t_p)|} |\kappa| d\xi_i(\tau) + \bar{b}, \tag{A1}$$

where $\bar{b} = \sup\{\sum_{i=j+1}^{n} \int_{\xi_i(0)}^{|\xi_i(t_p)|} (g_i(\tau)N(\xi_i(\tau)) + \kappa)d\xi_i(\tau) + \sum_{i=1}^{j} \int_{\xi_i(0)}^{0} (g_i(\tau)N(\xi_i(\tau)) + \kappa)d\xi_i(\tau) + b\}$. All $\xi_i(0)$ are given initial values meeting $\xi_i(0) \in \mathcal{L}_\infty$, so $\bar{b}$ is a positive constant.

By further scaling processing, one has

$$V(t_p) \leqslant \int_0^{\xi_\eta(t_p)} (\overline{g} j N^+(\xi_\eta(\tau)) - \underline{g} N^-(\xi_\eta(\tau)))d\xi_\eta(\tau) + \int_0^{\xi_\eta(t_p)} |\kappa| j d\xi_\eta(\tau) + \bar{b}. \tag{A2}$$

From property (ii), $\int_0^{l_p} N^-(\tau)d\tau$ is the high-order infinity relative to l_p and $\int_0^{l_p} N^+(\tau)d\tau$ for $l_p \to +\infty$. Since the higher order can absorb the lower order in the addition and subtraction rule of infinity, it can be concluded that $V(t_p) \to -\infty$ for $l_p \to +\infty$, which contradicts $V(t_p) \geqslant 0$. Thus, $\xi_\eta(t) \in \mathcal{L}_\infty$ and all $\xi_i(t) \in \mathcal{L}_\infty$ hold. For the other condition $g_i(t) < 0$, the boundedness of $\xi_i(t)$ can also be obtained by the same contradiction method, and the similar proof process is omitted. Thus, Case II does not exist.

Case III. All $\xi_i(t) \notin \mathcal{L}_\infty$ hold. As a special case, i.e., $j = n$ for Case II, it is also obtained that all $\xi_i(t) \in \mathcal{L}_\infty$, i.e., Case III does not exist.

Step 2. Suppose that all $\xi_i(t) \in \mathcal{L}_\infty$ for $t \in [T_{k-1}, T_k)$ $(k = 2, \ldots, +\infty)$, then $\lim_{t\to T_k^-} \xi_i(t) = \xi_i(T_k^-) \in \mathcal{L}_\infty$ holds.

Step 3. Owing to the continuity of $\xi_i(t)$, it yields $\xi_i(T_k) = \xi_i(T_k^-) \in \mathcal{L}_\infty$. Similar to the argumentation process in Step 1, it can be concluded that all $\xi_i(t) \in \mathcal{L}_\infty$ for $t \in [T_k, T_{k+1})$.

Based on the boundedness of $\xi_i(t)$ $(t \in [0, +\infty))$, it can be proven that $V(t)$ and $\sum_{i=1}^{n} \int_0^t (g_i(\tau)\mathcal{N}(\xi_i(\tau)) + \kappa)\dot{\xi}_i(\tau)d\tau \in \mathcal{L}_\infty$ for $t \in [0, +\infty)$.